Science Advances
AAAS

Supplementary Materials for

Metal-organic frameworks tailor the properties of aluminum nanocrystals

Hossein Robatjazi, Daniel Weinberg, Dayne F. Swearer, Christian Jacobson, Ming Zhang, Shu Tian, Linan Zhou, Peter Nordlander, Naomi J. Halas*

*Corresponding author. Email: halas@rice.edu

The PDF file includes:

Other Supplementary Material for this manuscript includes the following:

Movie S1 (.avi format). 3D reconstruction of Al NC@MIL-53(Al) particle morphology using electron tomography.

a)

b)

c)

Fig. S1. Crystal structure of the MIL-53(Al) MOF formed around Al NC. Crystal structure of the

MIL-53(Al) MOF rendered along different axes.
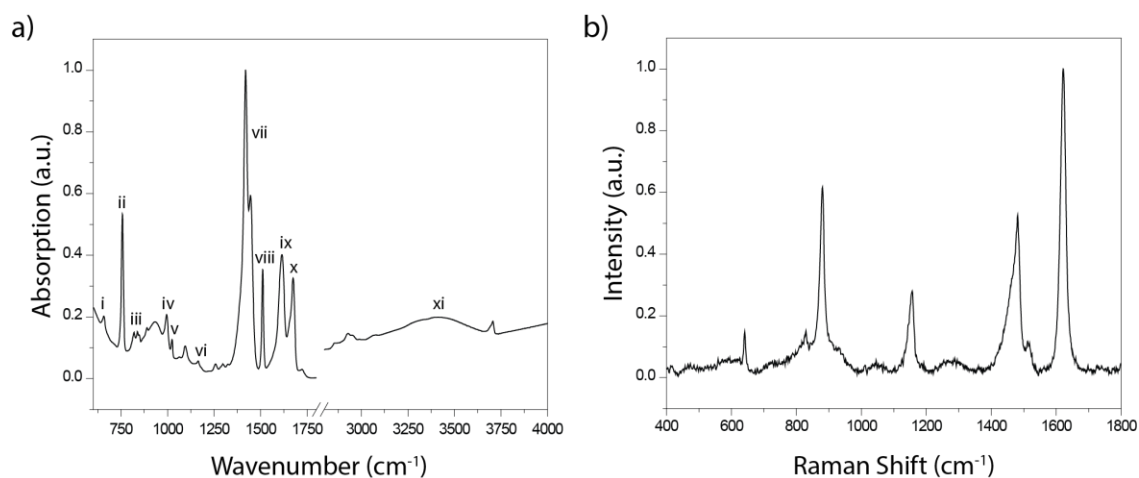
Fig. S2. Vibrational spectroscopy of the MIL-53(Al) framework surrounding Al NC core.

Vibrational spectra of MIL-53(Al) surrounding Al NC core**.** (a) FT-IR spectra and (b) Raman spectra of the Al@MIL-53(Al). In FT-IR spectra, peak (i) is attributed to the symmetric/antisymmetric stretch of the aluminum-oxide backbone. Peak (ii) at 760 cm^{-1} is attributed to the out-of-plane vibration of hydrogen atoms on the aromatic ring. Peak (iii) is attributed to the bend of the carboxyl group + bend of the aromatic ring. Peak (iv) corresponds to the rocking of the hydroxyl group. Peak (v) is the bending of the aromatic ring + rocking of hydrogen atoms on the aromatic ring. Peak (vi) is the stretch between the aromatic ring and carboxyl group + rocking of hydrogen atoms on the aromatic ring. Characteristics symmetric stretching vibrations (v_s) of the coordinated carboxylate groups is observed at around 1440 cm^{-1} and 1410 cm^{-1} (vii) and antisymmetric stretch (v_{as}) appears at 1620 cm^{-1} (ix). Stretch between the aromatic ring and carboxyl group + rocking of hydrogen atoms on the aromatic ring appears at around 1500 cm^{-1} (viii). The peak at 1660 cm^{-1} (x) corresponds to the C=O vibration of the DMF molecule trapped in MOF structure. Hydrogen-bonded water or DMF molecule appears at the region above 2000 cm-1 with the maximum at 3400 cm^{-1} (xi).The symmetric stretching vibration of the non-coordinating carboxylic group (if it existed) should appear at 1722 cm^{-1} and 1750 cm^{-1}. The absence of such vibrational characteristics indicates that the MOF structure does not have contamination from free linker molecules. The complementary vibrational active modes of MIL-53(Al) can be observed in Raman spectra of MIL-

53(Al) surrounding Al core. Both IR and Raman spectra of are well-matched with the vibrational

fingerprint of MIL-53(Al) in literature. (*43*)
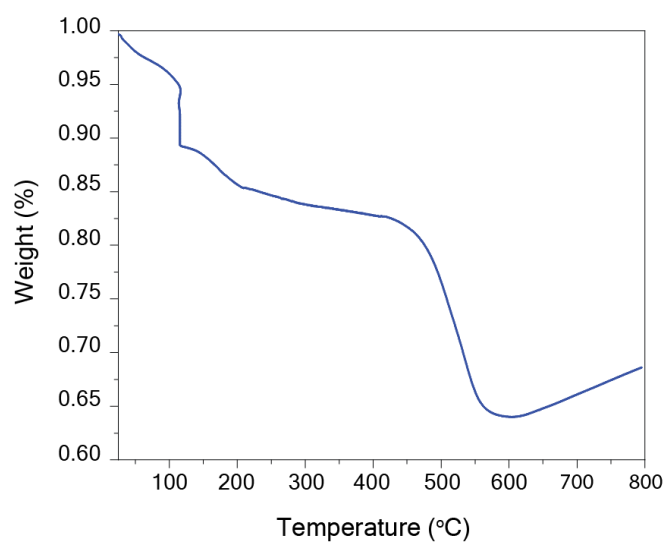
Fig. S3. TGA analysis of Al NC@MIL-53(Al). Thermogram of Al NC@MIL-53(Al) powder

under Argon flow. The weight loss below200 ^{o}Ccorresponds to the solvent (water and DMF)

removal. The sharp weight loss near 450 ^{o}C is attributed to the decomposition of the MIL-

53(Al). (*29*)

a

b
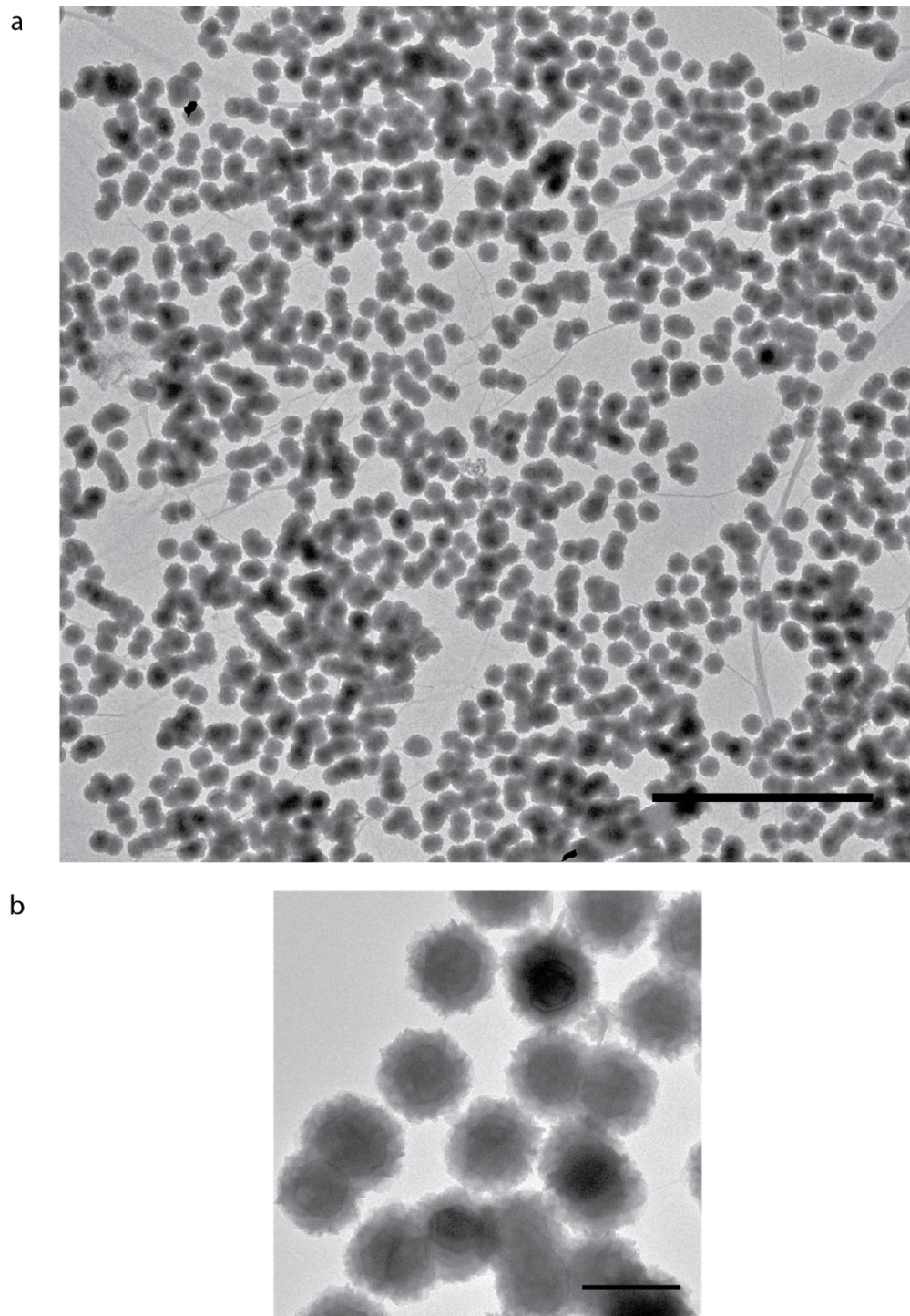
Fig. S4. Transmission electron microscopy characterizations of pristine Al NCs and Al NC@MIL-53(Al). Al NC@MIL-53(Al) hybrid plasmonic heterostructure (a) TEM image of the several particles over the large area (scale bar is 2 µm), and (b)representative TEM image of several particles at higher magnifications(scale baris 200 nm).
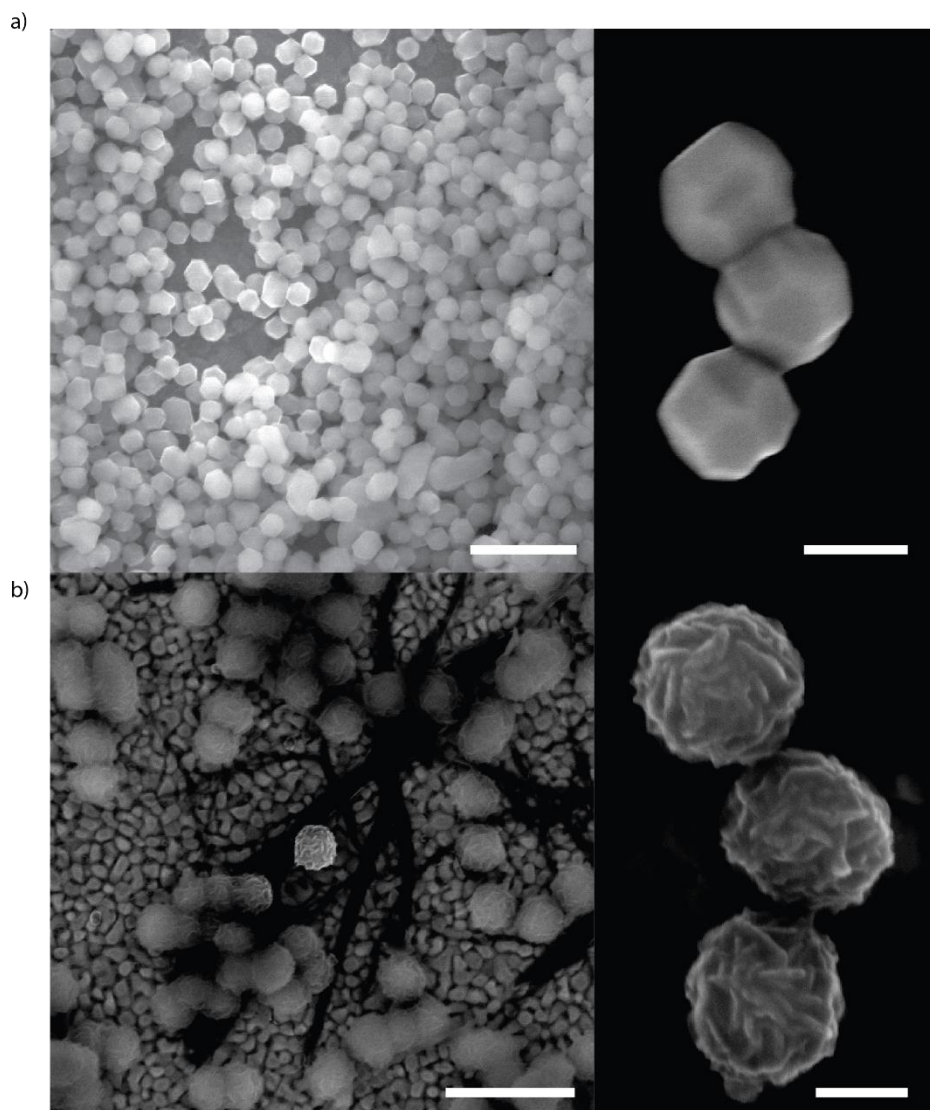
Fig. S5. Scanning electron microscopy characterizations of pristine Al NCs and Al NC@MIL-53(Al). SEM images of (a) pristine Al NCs at different magnifications (scale bars are 2μm and 100 nm) and Al NC@MIL-53(Al) (on conductive substrate)at different magnifications (scale bars are 500 nm and 100 nm). The small grains outside of the Al@MIL-53(Al) particles in (b) belong to the conductive substrate used for imaging. Significant changes to the particles surface morphology can be observed after MOF shell growth around the Al NCs core.
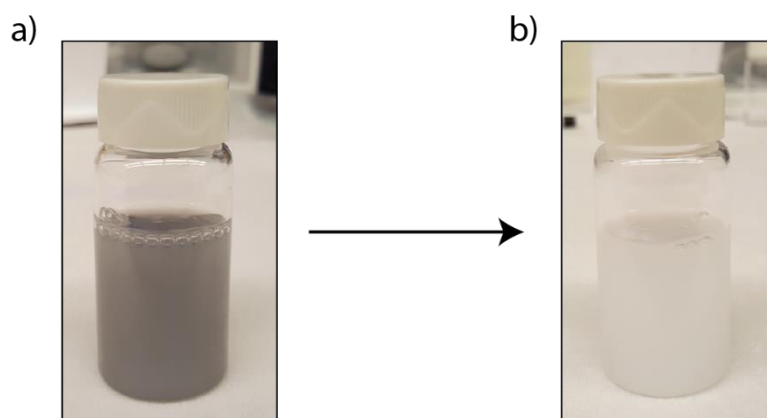
Fig. S6. Attempt for the synthesis of MIL-53(Al) shell around Al NCs following previously established synthetic strategy. Formation of the MIL-53(Al) shell around Al NCs does not proceed through previously established synthetic strategy for this MOF. (*29*) (a) Al NC (2 mg) mixture with Al $(NO_3)_3$ (15 mg) precursor and H_2BDC linker (5 mg/ml) in 12 ml of 50-50 DMF-H_2O solvent before (a) and after (b) 4 hours of incubation at 150^oC in an autoclave. The mixture was turned to white shortly after the reaction was initiated, indicating complete decomposition of Al NCs under reaction conditions to aluminum oxides.
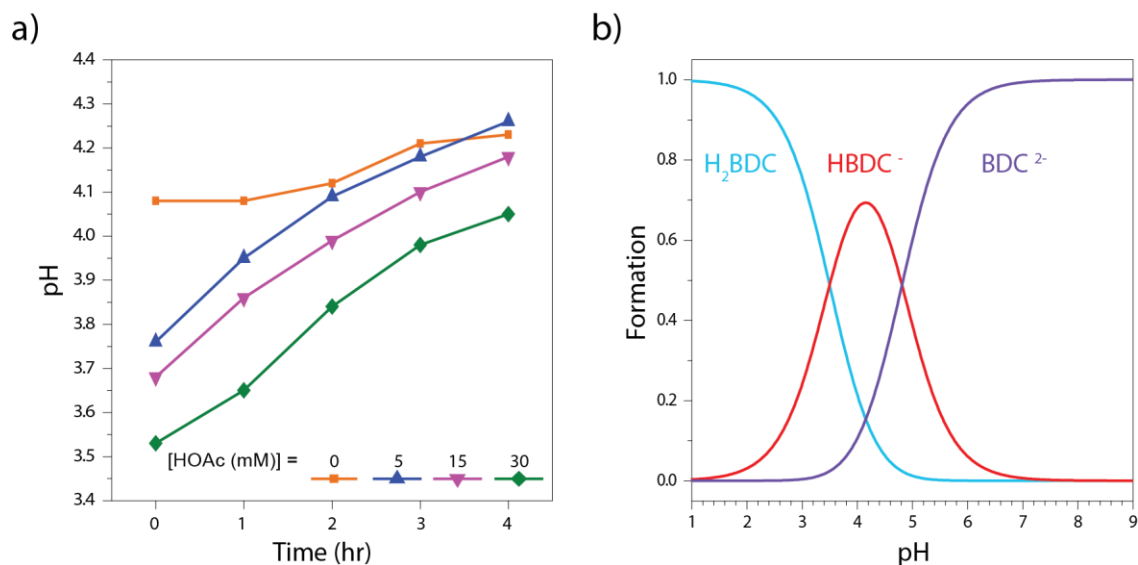
Fig. S7. Influence of the initial pH of the solution on formation of MIL-53(Al) around Al NCs. (a) pH variation during MIL-53(Al) growth around Al core carried out in presence of various concentration of acetic acid in the initial reaction mixture. (b) Variation of forms of benzene-1,4-dicarboxylic acid (H$_2$BDC) species as function of pH calculated from its pK$_a$ values (pK$_{a1}$ = 4.82, pK$_{a1}$ = 3.51). Addition of increasing quantities of the acid lowers the initial pH of the reaction mixture that consequently increases the rate of Al dissolution but suppresses formation of deprotonated forms of the linker (BDC^{-2}) required for MOF nucleation and growth. Consumption of [H$^+$] as the dissolution step proceeds causes a gradual increase of the mixture pH and formation of linker anions that favors MOF crystal nucleation and growth.
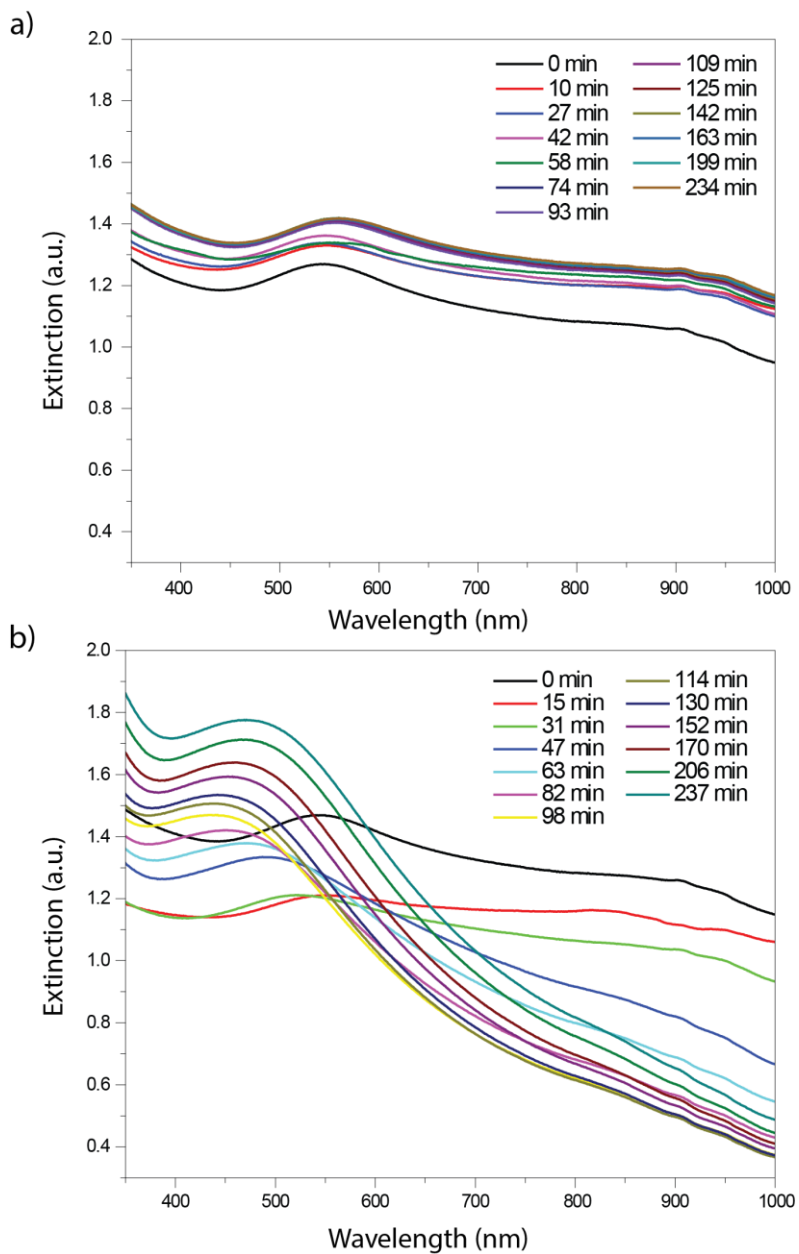
Fig. S8. Time-dependent UV-Vis extinction spectrum of the reaction mixture during MIL-53(Al) shell formation around Al NCs. (a) Under typical reaction conditions in the absence of acetic acid (b) in the presence of 3.66 mmolacetic acid added to the initial reaction mixture (acid to linker ratio of 30). See the main text for furtherexplanation.
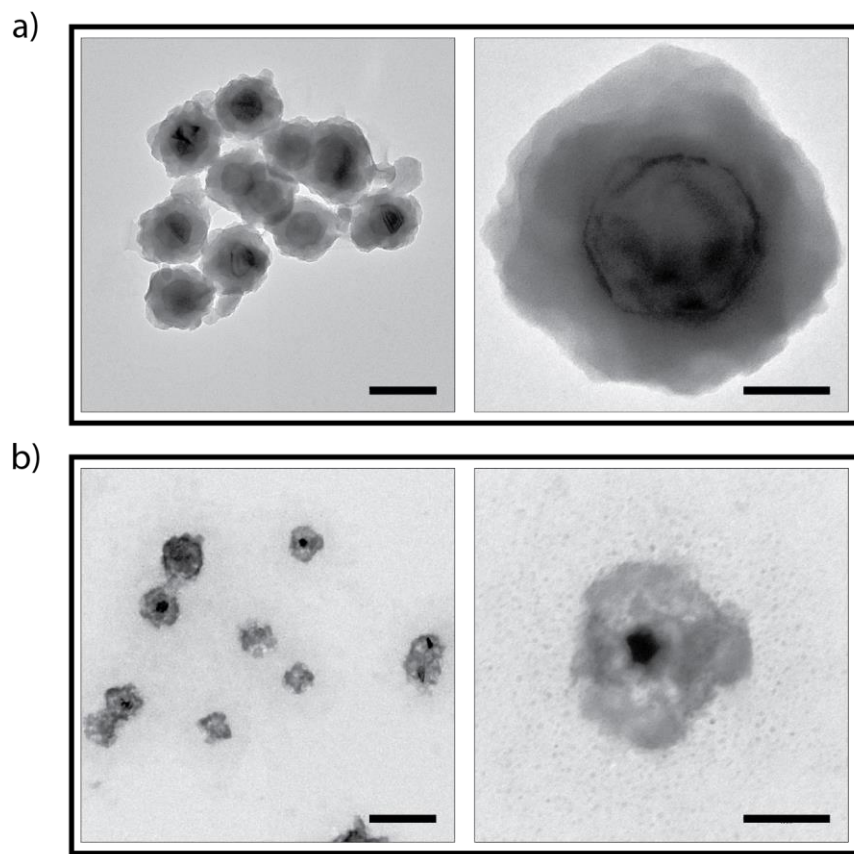
Fig. S9. The role of organic linker on establishing MOF shell during hydrothermal dissolution of Al NC. H_2BDC linkerinhibits Al NCs from complete dissolution under reaction conditions by establishing a MOF shell around Al core. (a) TEM images of the several and a single Al NC@MIL-53(Al) hybrid obtained from the reaction mixture containing H_2BDC linker and 30 mM of acetic acid. (b) TEM images of the Al NCs incubated under the same reaction condition as (a) but in the absence of the organic linker showing nearly complete dissolutionof NCs within the reaction timescale. The dissolved metallic Al appears as a ghost oxide layeraround the remaining Al core(Scale bars are 200 nm, and 50 nm for several and single particle images, respectively).
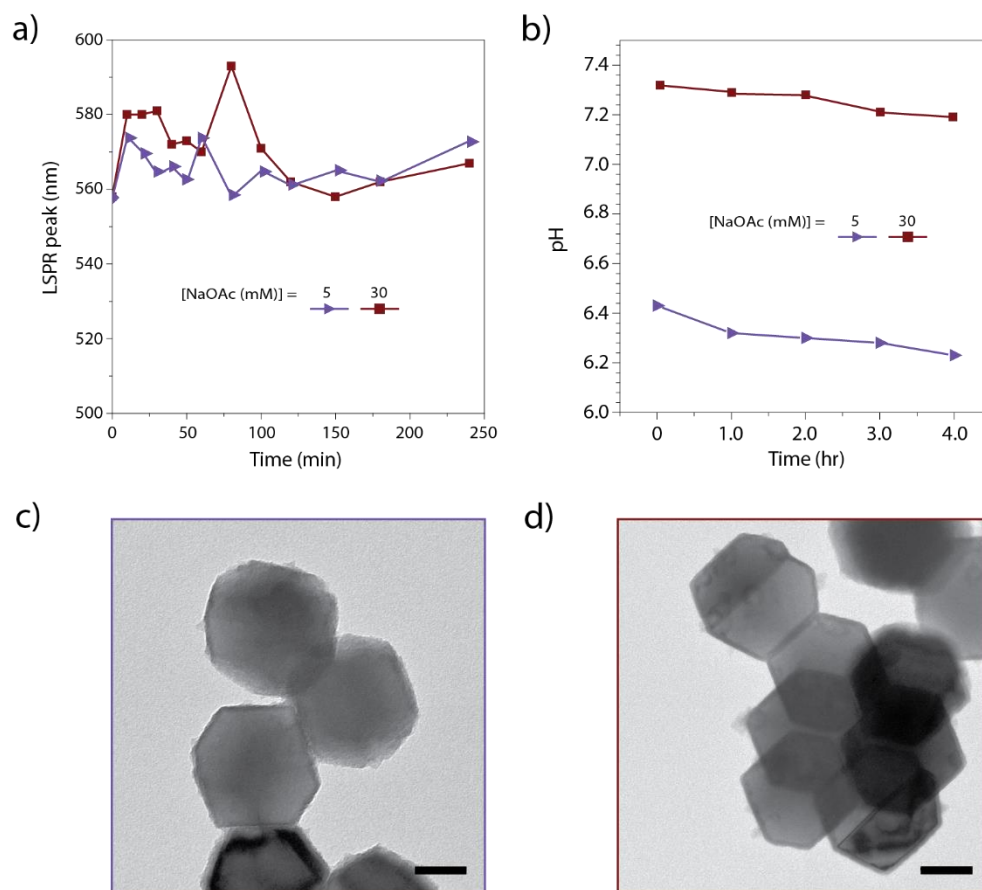
Fig. S10. Influence of sodium acetate on MOF formation progress. The addition of sodium acetate (NaOAc) to the reaction mixture inhibited MIL-53(Al) growth around Al core. (a) LSPR of the Al core and (b) pH variation during the reactions performed in the presence of 5mM and 30 mMof NaOAcin the initial reaction mixture. (c,d) Representative TEM images of the particles after the reaction in the presence of 5mM (c) and 30 mM (d) of showing lackof MOF growth. In contrast to the addition of acetic acid, the LSPR of the Al core does not show any blue-shift or red-shift trend in presence of various quantities of sodium acetate. Compared to the higher acidity of the reaction mixture in the presence of the acetic acid that favors Al dissolution and MOF formation in the presence of very low concentration of the linker anions, the nearly neutral pH of the mixture in the presence of sodium acetate significantly suppress the dissolution of Al core, and inhibits MOF growth despite higher concentration of the linker anions at this pH.
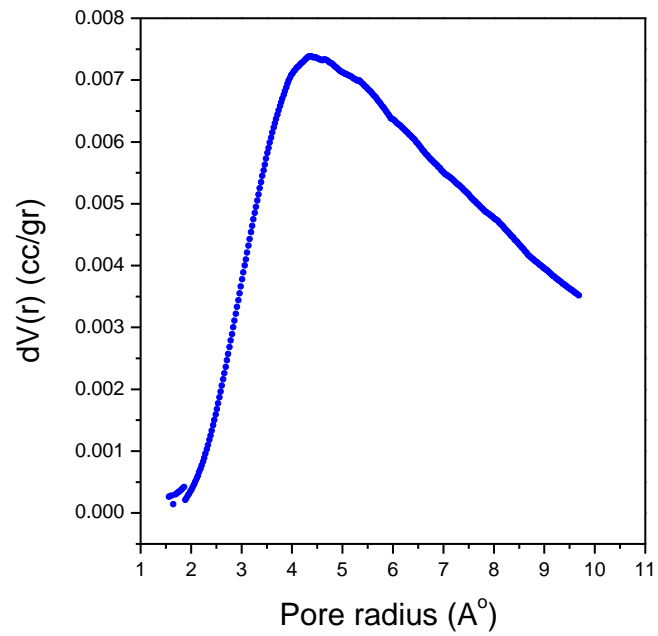
Fig. S11. Pore size distribution of MIL-53(Al) shell layer around Al NC core. The data were calculated based on the results of sorption experiment in Fig. 5a using Horvath-Kawazoe (HK) method.
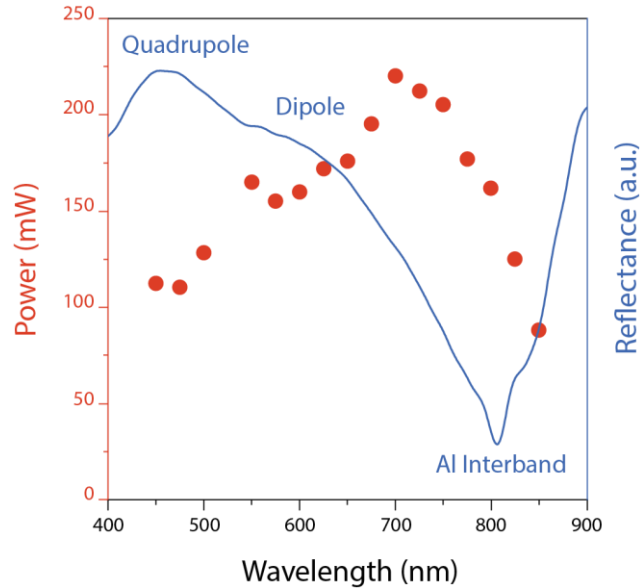
Fig. S12. Spectrum of the light source used for photocatalysis and optical characterization of Al NC@MIL-53(Al) on γ-Al₂O₃ support. The emission spectrumof the white light laser source used for photocatalytic characterizations (red); and diffuse reflectance spectrum of Al NC@MIL-53(Al) on γ-Al₂O₃support in the air (blue line) showing the dipolar and quadrupole plasmon resonance feature and interband absorption of the Al core.
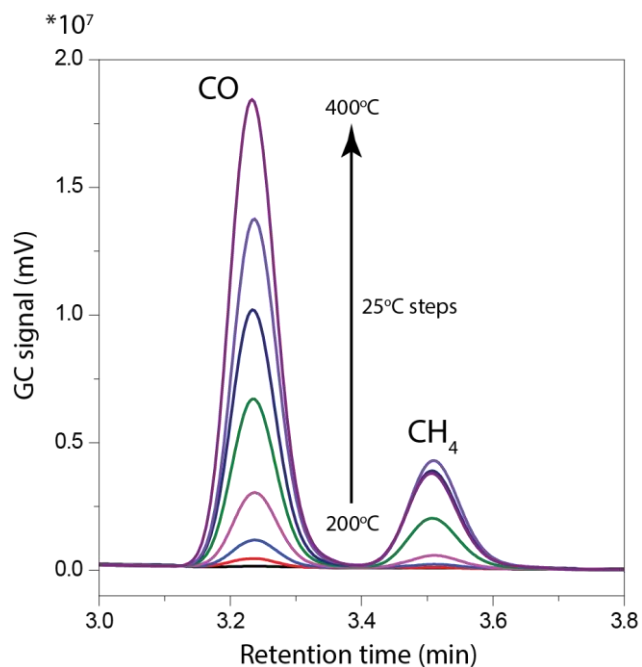
Fig. S13. Product selectivity for thermally driven rWGS. Typical gas chromatogram of thechamber output during thermal driven rWGS on Al NC@MIL-53 (Al) at the range of 200°C to 400°C showing the formation of CO and CH_4 as reaction products (1:1 ratio of CO_2:H_2 continuously flowed into the reaction chamber at a total flow rate of 20 s.c.c.m.).

a)

b)

c)

Al NC@[Al(OH)(1,4-ndc)]$_n$

Al NC

2Theta (degree)

d)

Z
Y

Z
X

X
Y
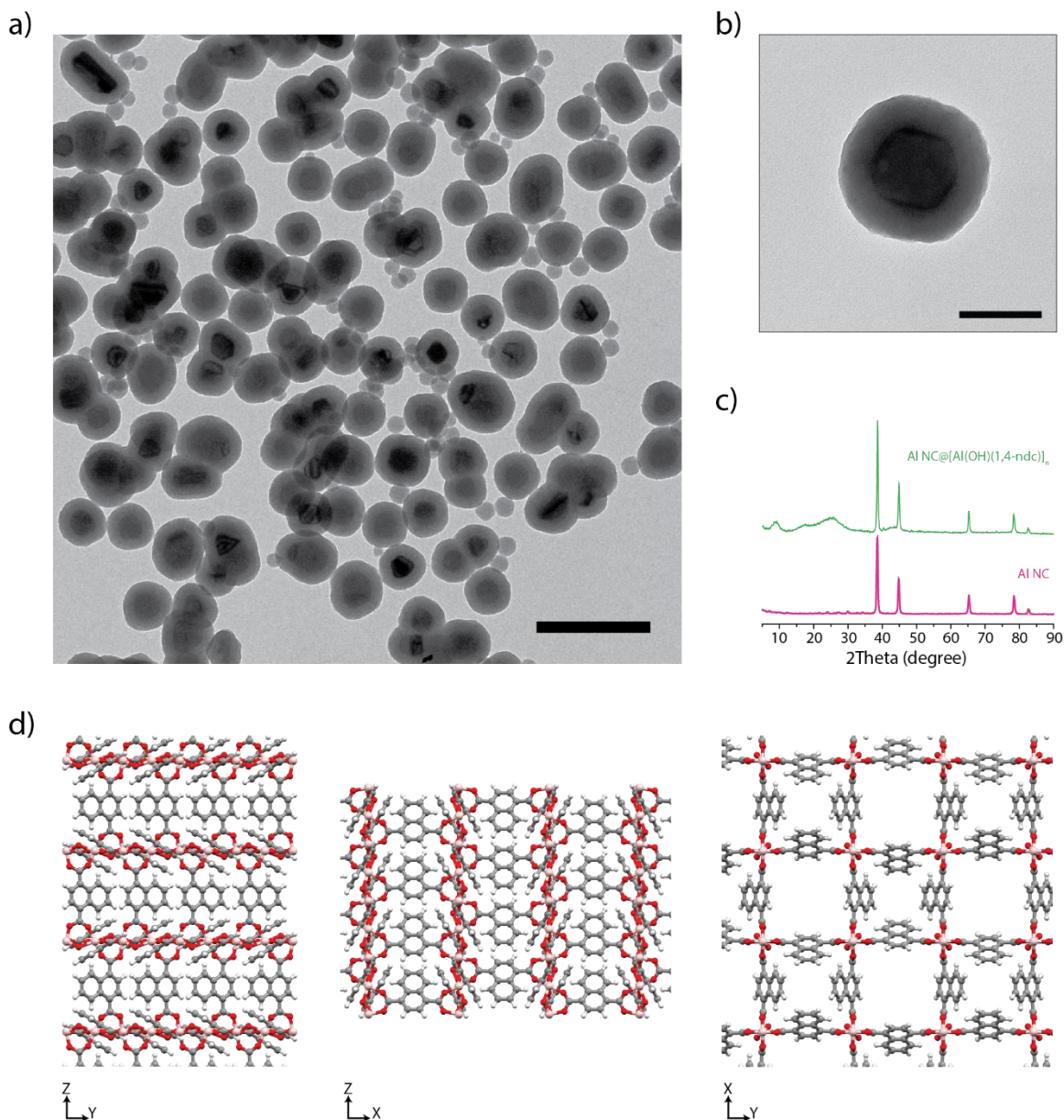
Fig. S14. Applying the dissolution-and-growth approach to Al NCs in a solution of 1,4-NDC.

Applying dissolution-and-growth approach to Al NCs in a solution of 1,4-naphthalenedicarboxylic

acid(1,4-NDC) as an organic linker. TEM images of the several (a) and a single (b) hybrid nanoparticle

show formation of highly conformal MOF shell surrounding the individual Al cores (scale bars are

500nm and 100 nm, respectively). (c) Powder X-ray diffraction pattern of MOF-coated particles

compared to pristine Al NCs. The existence of the [Al(OH)(1,4-ndc)]$_n$ can be confirmed by comparison of

the pattern at the range of $2\theta = 5^{o}\text{-}35^{o}$ with the simulated and experimental results of this MOF in the

literature (*44*). However, the diffraction peaks in MOF region are broad that indicates small crystalline domain size of the MOF shell grown from amorphous surface oxide of aluminum. Future optimization of the reaction condition may improve the crystallinity of the MOF shell layer. (d) Crystal structure of the known [Al(OH)(1,4-ndc)]$_n$ illustrated along the different axis (from left to right axis-X to axis-Z).
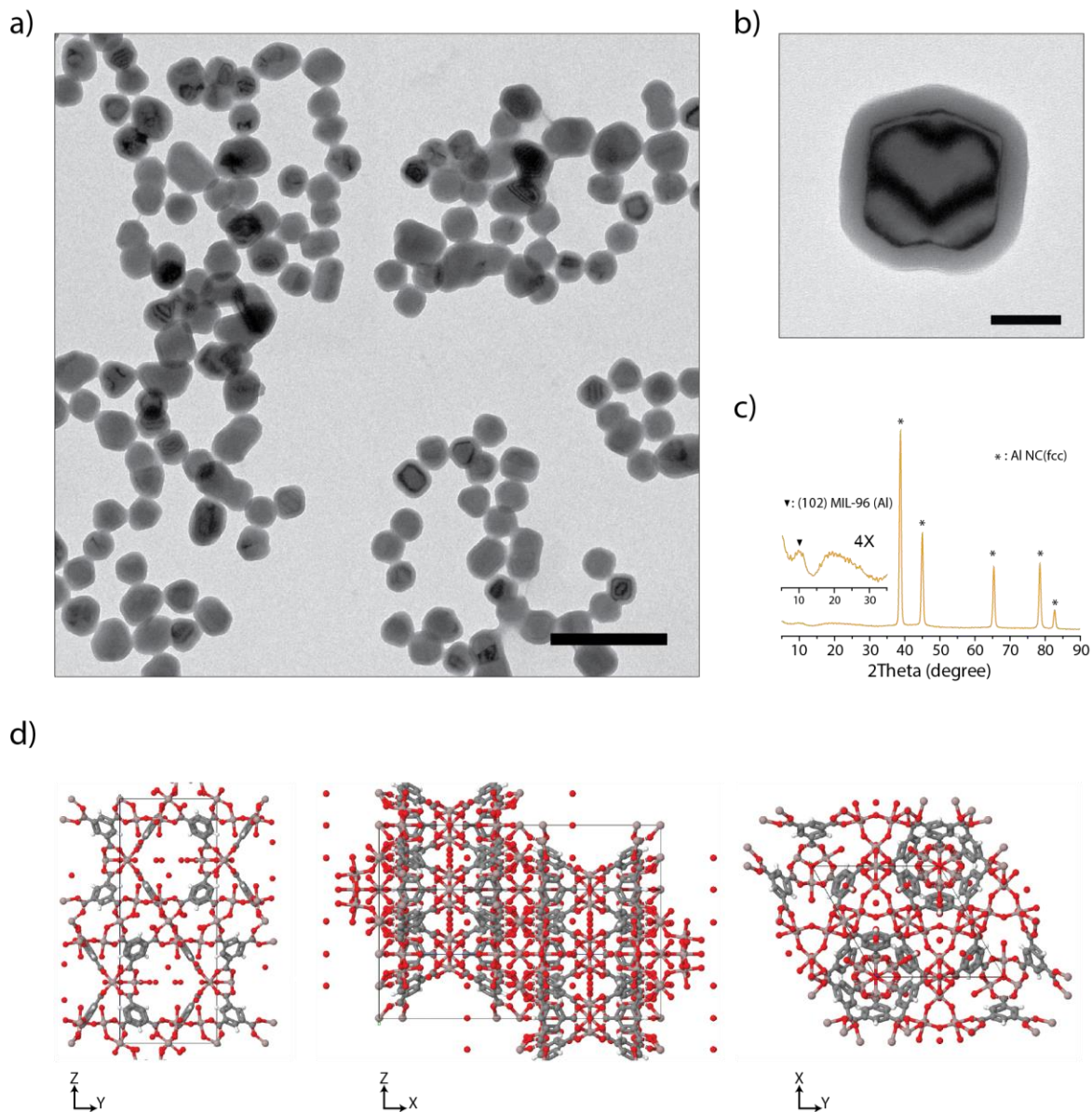
a)

b)

c)

d)

Fig. S15. Applying the dissolution-and-growth approach to Al NCs in a solution of H₃BTC.

Applying dissolution-and-growth approach to Al NCs in a solution of Benzene-1,3,5-tricarboxylic acid

(H₃BTC) as an organic linker. TEM images of the several (a) and a single (b) hybrid nanoparticle show

formation of highly conformal MOF shell surrounding the individual Al cores (scale bars are 500nm and

100 nm, respectively). (c) Powder X-ray diffraction pattern of MOF-coated particles compared to pristine

Al NCs. A comparison of the diffraction pattern at the range of $2\theta = 5^{o}\text{-}35^{o}$ with the simulated and

experimental results in the literature (*45*) revealed that the MOF shell likely exists in the form of MIL-96

(Al) framework ($Al_{12}O(OH)_{18}(H_2O)_3(Al_2(OH)_4)[btc]_6·24H_2O$). Broad features in the MOF region are assigned to multiple relatively intense or weak diffraction peaks corresponding to (102), (112), and (200) to (204) lattices with small crystalline domain sizes of the MOF shell. Future optimization of the reaction condition may improve the crystallinity of the MOF shell layer. (d) Crystal structure of the known MIL-96 (Al) illustrated along the different axis (from left to right axis-X to axis-Z).

Al NCs suffer from poor stability in aqueous environment that limits their implementation in many traditional plasmonic applications. We demonstrate that rational functionalization of the surface of the nanocrystals with $[Al (OH)(1,4\text{-}ndc)]_n$ shell can significantly improve their stability in water owing to hydrophobic characteristics of this MOF.

The TEM images of the particles obtained after two days of incubation in water revealed partial oxidation of the bare Al NCs whereas Al core in $Al@[Al (OH)(1,4\text{-}ndc)]_n$ hybrid remained completely intact (fig. S16). After four days of incubation, the bare Al NCs are completely oxidized, but the Al core in Al@NDC MOF hybrid particles remains fine although structural deformation of MOF layer around Al NCs is observed. The enhanced stability of the Al@MOF hybrid is also confirmed by the stable optical feature in obtained extinction spectrum of the particles solution. A comparison of the normalizedUV-Vis extinction spectrum of pristine particles and after 4 days of incubation in water shows complete disappearance of the dipolar plasmon mode (at 440 nm) of the bare Al NCs indicating complete oxidation of nanocrystal. In contrast,the resonance feature of the MOF-coated particles does not show a major change indicating little to no oxidation of the Al core. The aqueous solution of bare particles after complete oxidation at day four turned white (inset digital image in (a)), compared to the vibrant

color of the aqueous solution MOF-coated particles resistant to oxidation (inset digital image (b)).
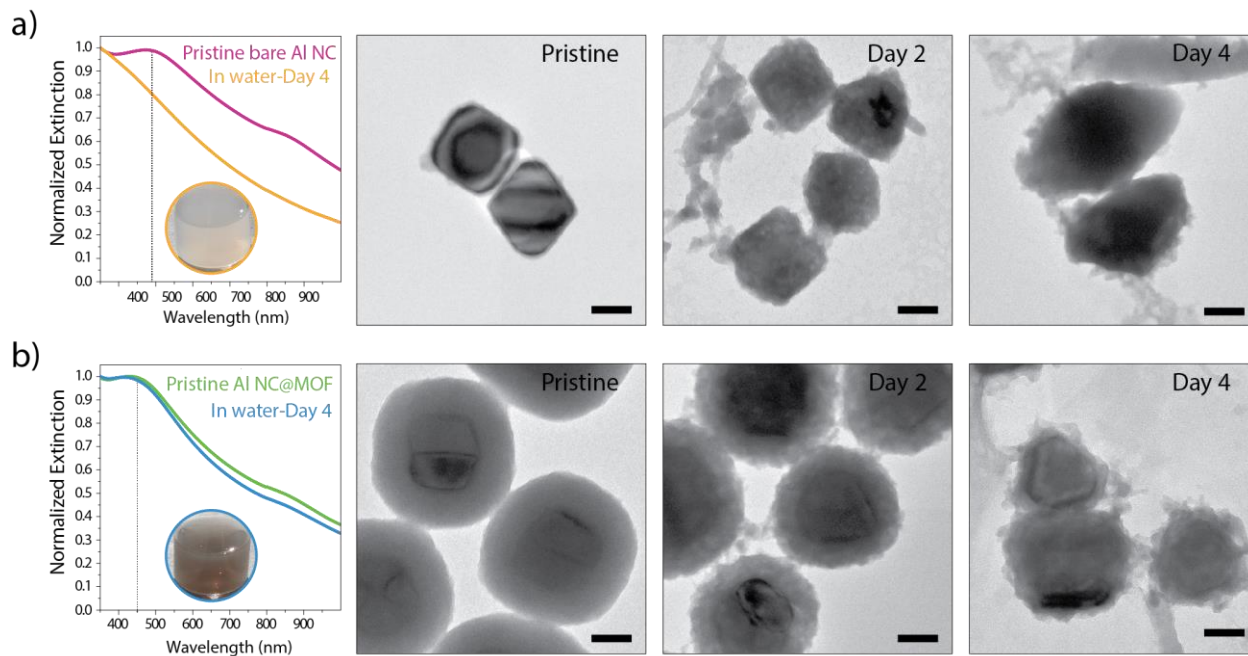
Fig. S16. Enhanced stability of Al NC in water through rational MOF coating. a) Normalized UV-Vis extinction spectrum and corresponding TEM images of the (a) bare and (b) $[Al (OH)(1,4\text{-}ndc)]_n-$ coated Al NCs in water. The aqueous solution of bare nanocrystals turned to white (inset digital image in (a)) after four days in water along with complete disappearance of the dipolar LSPR maximum (around 440 nm) in the UV-Vis extinction spectrum, indicating nanocrystal oxidation. Complete oxidation of the nanocrystals is also confirmed by TEM images. In contrast, MOF-coated particles showing resistivity to oxidation due to the hydrophobic characteristics of the MOF layer. The TEM images show that the Al core in theAl@MOF hybrid remained nearly intact after 4 days of incubation in water. The resonance feature of the aqueous solution of the MOF-coated particles at 450 nm does not show a major change,indicating little to no oxidation of the Al core. The inset in (b) is the digital image of the aqueous solution ofMOF-coated particles at day 4.Scale bars are 50 nm.

Combination of plasmonicnanoantennas with active transition metal-based catalysts is known as "antenna-reactor" nanostructures (*24*).By coupling to the Al NC, the light absorption in small decorating TM islands can be significantly increased. Rational combining of the antenna-reactor photocatalyst complexes with MOF has enormous potential to greatly expand the scope of the plasmon-mediated chemical reactions whose efficiencies and selectivities can be improved. Here we show an example of the "antenna-reactor" complex based on Al NC that is surface functionalized with the MOF shell.

a)

Al NC@Pt

b)

Al NC@Pt@MIL-53
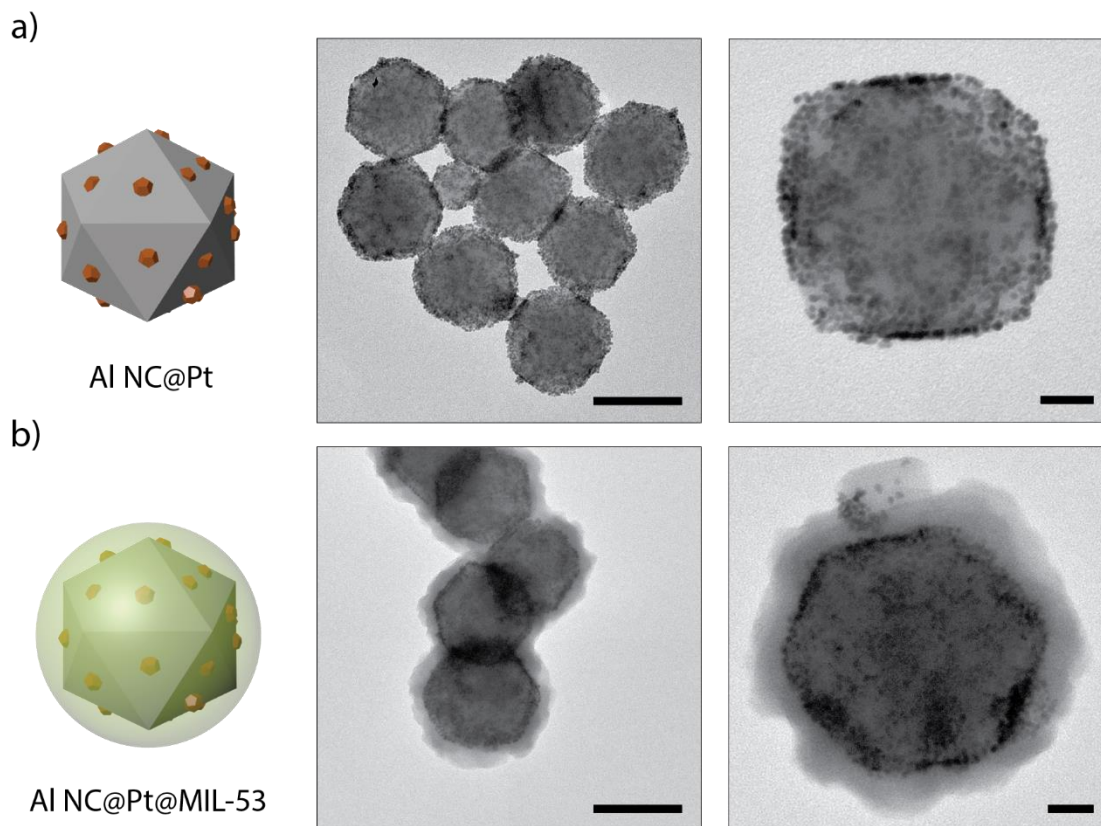
Fig. S17. Coupling catalytically active TM nanoparticle islands to the Al@MOF hybrid for future photocatalytic applications. Transition metal-decorated Al NC@MOF heterostructure. a) TEM images of the several Al-Pt NPs (left, scale bar is 100 nm) and a single Al-Pt NP (right, scale bar is 20 nm) decorated with high coverage of Pt islands (about 3 nm in size). Particles were synthesized according to our previously publishedprotocol with minor modifications (*39*).b) TEM images of the several Al-

Pt@MOF hybrid (left, scale bar is 100 nm) and a single Al-Pt NP@MOF (right, scale bar is 20 nm) after MIL-53(Al) MOF shell growth. The MOF shell growth was performed using the dissolution-and-growth of the native oxide layer as explained in the main text.